

# Dielectric response effects in attosecond time-resolved streaked photoelectron spectra of metal surfaces

C.-H. Zhang and U. Thumm

*Department of Physics, Kansas State University, Manhattan, Kansas 66506, USA*

(Dated: October 29, 2018)

The release of conduction-band electrons from a metal surface by a sub-femtosecond extreme ultraviolet (XUV) pulse, and their propagation through the solid, provokes a dielectric response in the solid that acts back on the photoelectron wave packet. We calculated the (wake) potential associated with this photoelectron self-interaction in terms of bulk and surface plasmon excitations and show that it induces a considerable, XUV-frequency-dependent temporal shift in laser-streaked XUV photoemission spectra, suggesting the observation of the ultrafast solid-state dielectric response in contemporary streaked photoemission experiments.

PACS numbers: 78.47.J-, 42.65.Re, 79.60.-i,

The sudden release and subsequent motion of a photoelectron (PE) in and in front of a solid dielectric medium provokes collective electron excitations in the solid. The back-interaction of these excitations with the PE can be modeled as a dynamic, wave-like redistribution of electronic density in the solid in terms of a complex-valued effective electron-self-interaction (or “wake”) potential [1–4]. This density wake appears since the electron distribution in the solid cannot equilibrate during the motion of the released electron. The wake potential depends on the kinetic energy  $E$  of the PE. Its real part is due to virtual excitations of bulk and surface plasmons, while its imaginary part accounts for inelastic scattering and energy loss. The dependence of the dynamic wake potential on the charge state and velocity of a classical particle has been studied extensively over several decades with regard to energy loss [5, 6], electron-exchange and -correlation contributions [7], electron emission in ion-surface collisions [8], and electronic self-interaction effects on photoelectron spectra [9]. While these examples emphasize the influence of the solid’s dielectric response, they do not resolve the ultrafast electronic response in the condensed-matter-plus-charged-particle system in time. Owing to significant progress in laser technology over the past decade, sub-femtosecond XUV pulses can now be generated and synchronized with the primary IR laser pulse, allowing the time-resolved observation of the electronic dynamics in atoms [10] and solids [11]. Time-resolved experiments at the intrinsic time-scales of an active electron and the correlated dynamics of two electrons [12, 13] or plasmons [14, 15] promise unprecedented sensitive experimental tests of collective electronic transport phenomena in solids and novel plasmonic devices [16, 17].

Using attosecond time-resolved XUV+IR pump-probe technology in a proof-of-principle experiment, a relative temporal shift of 110 as (1 as =  $10^{-18}$  s) between the photoemission of 4f core level and conduction-band electrons from a tungsten (110) surface was measured [11]. Essential for the correct reproduction of this shift within simple quantum mechanical models [18, 19] is the proper inclu-

sion of (i) the PE’s phase evolution during the streaked emission, (ii) the attenuation of the IR pulse inside the solid (skin effect), and (iii) electron transport effects in the solid. The phase of the PE is further affected by its plasmon-mediated self-interaction while moving inside and outside the solid, and we expect streaked photoemission experiments to help reveal these dynamic many-body effects in solids. In this Letter we investigate how these three factors affect the PE dynamics and extend previous theoretical studies on the streaked photoemission from solid surfaces [18, 20–22] to expose the effect of the dynamic plasmon response on time and energy resolved PE spectra.

We calculate the dynamic wake potential assuming that the released PE moves with a constant velocity  $v_z > 0$  along a classical trajectory towards and perpendicular to the surface and crosses the metal-vacuum interface ( $z = 0$ ) at time  $t = 0$ , leading to the density  $\rho(\mathbf{r}) = \delta(\mathbf{r}_{\parallel})\delta(z - v_z t)$  (throughout this Letter we use atomic units, unless stated otherwise). The semi-infinite solid is modeled in jellium approximation [18], and its excitations are described by the dispersion relations for bulk- and surface-plasmon excitations,  $\omega_k^2 = \omega_p^2 + 3k_F^2 k^2/5 + k^4/4$  and  $\omega_Q^2 = \omega_s^2 + \sqrt{3}k_F\omega_s Q/\sqrt{5} + \beta Q^2 + Q^4/4$  [4, 23]. For low momenta  $\mathbf{k} = (\mathbf{Q}, k_z)$ , these relations model single-plasmon modes with bulk- and surface-plasmon frequencies  $\omega_p^2 = 4\pi n$  and  $\omega_s = \omega_p/\sqrt{2}$ , respectively, and decay into particle-hole excitation at high momenta through the terms  $k^4/4$  and  $Q^4/4$ .  $n$  is the bulk-conduction-electron density, and  $k_F = (3\pi^2 n)^{1/3}$  is the Fermi velocity.  $\beta$  is determined so that the surface-plasmon dispersion relation joins the particle-hole continuum at the same point as the bulk line [23]. The plasmon field of the solid is then given by the Hamiltonian  $H_0 = \sum_{\mathbf{Q}, k_z \geq 0} \omega_k b_{\mathbf{k}}^\dagger b_{\mathbf{k}} + \sum_{\mathbf{Q}} \omega_Q a_{\mathbf{Q}}^\dagger a_{\mathbf{Q}}$ , where  $b_{\mathbf{Q}}^{(\dagger)}$  and  $a_{\mathbf{k}}^{(\dagger)}$  are annihilation (creation) operators for bulk and surface plasmons, respectively [5, 7, 9]. The interaction between the PE and the jellium solid is given by  $H_1 = \int d\mathbf{r} \rho(\mathbf{r}) [\phi_b(\mathbf{r}) + \phi_s(\mathbf{r})]$ , where  $\phi_b(\mathbf{r}) = \sum_{\mathbf{Q}, k_z \geq 0} B_{\mathbf{k}} b_{\mathbf{k}} \sin(k_z z) e^{i\mathbf{Q}\cdot\mathbf{r}_{\parallel}} \Theta(-z) + \text{h.c.}$

and  $\phi_s(\mathbf{r}) = \sum_{\mathbf{Q}} A_{\mathbf{Q}} a_{\mathbf{Q}} e^{-Q|z|} e^{i\mathbf{Q}\cdot\mathbf{r}_{\parallel}} + \text{h.c.}$  are the bulk and surface plasmon fields.  $|B_{\mathbf{k}}|^2 = 8\pi\omega_p^2/(Vk^2\omega_k)$  and  $|A_{\mathbf{Q}}|^2 = \pi\omega_s^2/(SQ\omega_Q)$  are the interaction strengths (with quantization volume  $V$  and surface  $S$ ) [7].

The wavefunction  $|\psi(t)\rangle$  of the bulk and surface plasmon field interacting with the classical charged particle

$$V_{im}^r(z, v_z) = \frac{\Theta(-z)\omega_p^2}{\pi} \int_0^\infty \frac{dk}{k} \int_0^k dk_z \frac{(k_z^2 v_z^2 - \omega_k^2)[1 - \cos(2k_z z)]}{(k_z^2 v_z^2 - \omega_k^2)^2 + k_z^2 v_z^2 \gamma^2} - \Theta(z)v_z\omega_s^2 \int_0^\infty dQ Q \frac{e^{-Qz}}{\omega_Q} \frac{\sin(\omega_Q z/v_z)}{Q^2 v_z^2 + \omega_Q^2} - \frac{\omega_s^2}{2} \int_0^\infty dQ \frac{e^{-2Q|z|}}{Q^2 v_z^2 + \omega_Q^2}, \quad (1)$$

where  $\Theta(z)$  is the unit step function and  $\gamma$  the decay-width of the plasmon excitation. The first term in (1) includes bulk and the last two terms surface plasmon excitations.

Figure 1(a) shows  $V_{im}^r(z, v_z)$  for different PE velocities  $v_z$  for aluminum with  $\omega_s = 0.378$  [24], assuming  $\gamma = 0.1\omega_s$ . The static image potential is obtained in the limit  $v_z = 0$ . For  $v_z > 0$ ,  $V_{im}$  oscillates near the metal surface with wavelength  $\lambda_b = \pi v_z/\omega_p$  inside the solid and  $\lambda_s = 2\pi v_z/\omega_s$  in the vacuum, and approaches  $-1/4z$  [24] far away from the surface for all  $v_z$ , as expected. Equation (1) underestimates the influence of the positively charged ion cores, and its bulk limit ( $\approx 5.8$  eV) does not reproduce the Al Fermi energy ( $\varepsilon_F = 11.7$  eV) [25]. We therefore add a step potential to obtain the effective dynamic image potential,

$$U(z, v_z) = -\frac{V_0}{1 + e^{z/a}} + V_{im}(z, v_z) \quad (2)$$

and adjust the depth to  $V_0 = 11.7$  eV and interface-thickness parameter to  $a = 1.4 \text{ \AA}$ , respectively, in order to reproduce  $\varepsilon_F$  in the static limit for  $v_z = 0$  [Fig. 1(b)].

We model the metal surface as a 300 a.u wide slab and obtain its eigenvectors  $\varepsilon_n$  and wave functions  $\psi_n(z)$  by diagonalizing the time-independent Schrödinger equation (SE)

$$\varepsilon_n \psi_n(z) = \left[ -\frac{1}{2} \frac{d^2}{dz^2} + U(z, v_z = 0) \right] \psi_n(z). \quad (3)$$

In typical streaking experiments, the XUV pulse intensity is sufficiently low, so that photoemission in the XUV pulse  $E_X(t)$  can be treated perturbatively. The release and propagation of the PE wavepacket  $\delta\psi_n(z, t)$  from the state  $\psi_n(z, t)$  is then dictated by the SE [19]

$$i \frac{\partial}{\partial t} \delta\psi_n(z, t; \tau) = [H_L(t) + \delta U(z, v_z)] \delta\psi_n(z, t; \tau) + z E_X(t + \tau) \psi_n(z, t; \tau). \quad (4)$$

for the model Hamiltonian  $H = H_0 + H_1$  can be solved exactly [5, 6]. The wake potential of the PE is then calculated as  $V_{im}(t) = \frac{1}{2} \langle \psi(t) | H_{1,I}(t) | \psi(t) \rangle$ , where  $H_{1,I}(t)$  is the interaction-picture presentation of  $H_1$ . Following [4, 7, 23], we obtain the real part of wake potential

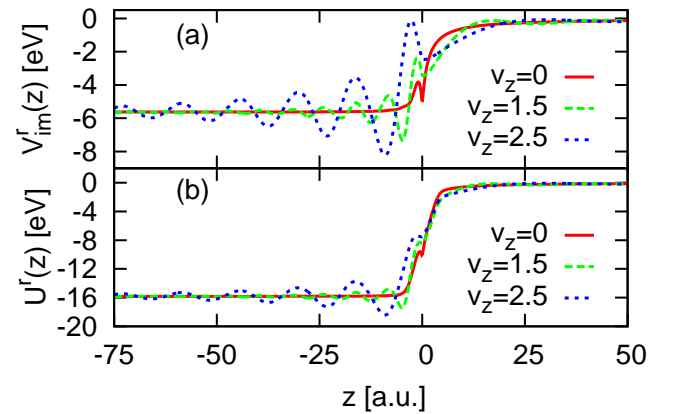


FIG. 1: (Color online) (a) Dynamic wake potential  $V_{im}^r(z, v_z)$  for Al for different PE velocities  $v_z$ . (b) Real part of  $U(z, v_z)$ , adjusted to the Fermi energy of Al at  $v_z = 0$ .

$H_L = \frac{1}{2} \left[ -i \frac{d}{dz} + A_L(z, t) \right]^2 + U(z, 0)$  is the Hamiltonian for the solid slab in the presence of the IR-laser pulse  $A_L(z, t)$ ,  $\tau$  the delay between the XUV and IR pulses with  $\tau > 0$  if the XUV precedes the IR pulse,  $\delta U(z, v_z) = V_{im}(z, v_z) - V_{im}(z, 0)$  represents the complex-valued dynamic part of the PE self-interaction, and  $v_z = \sqrt{2(\omega_X - |\varepsilon_n|)}$  is the PE speed. The evolution of the  $n$ -th initial state of the slab below the Fermi surface in the IR pulse is given by

$$i \frac{\partial}{\partial t} \psi_n(z, t) = H_L(t) \psi_n(z, t). \quad (5)$$

Since  $E_{L(X)}(t \rightarrow \pm\infty) = 0$ , (4) and (5) are solved for the initial conditions  $\delta\psi_n(z, t \rightarrow -\infty; \tau) = 0$  and  $\psi_n(z, t \rightarrow -\infty) = \psi_n(z) e^{-i\varepsilon_n t}$ .

We represent the vector potential of the laser pulse as  $A_L(t) = A_0 \sin^2(\pi t/\tau_L) \cos[\omega_L(t - \tau_L/2)]$  for  $0 \leq t \leq \tau_L$  and 0 otherwise, with  $\hbar\omega_L = 1.57$  eV, intensity  $I_L = A_0^2 \omega_L^2/2 = 5 \times 10^{11} \text{ W/cm}^2$ , and pulse length  $\tau_L = 8$  fs. We assume an exponential damping of the IR laser field inside the solid  $A_L(z, t) = A_L(t) [e^{z/\delta_L} \Theta(-z) + \Theta(z)]$

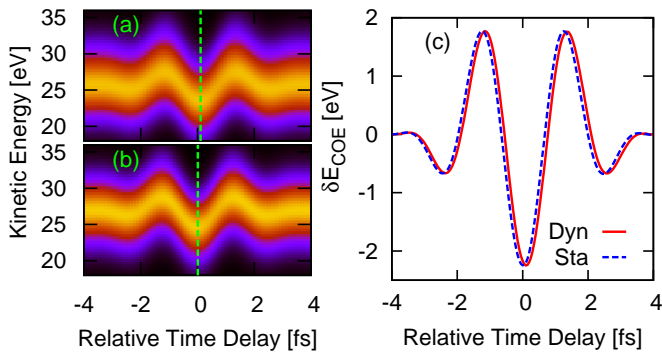


FIG. 2: (Color online) Streaked PE spectra for an Al surface calculated with the (a) dynamic image potential  $\delta U(z, v_z)$ , (b) static image potential  $\delta U(z, v_z = 0)$  for  $\hbar\omega_X = 40$  eV, skin depth  $\delta_L = 0$ , and mean free path  $\lambda = 5$  Å. (c) Corresponding center-of-energy shifts  $\delta E_{COE}$ . The temporal shift between the traces  $\delta E_{COE}$  for dynamic and static image potentials is  $\approx 100$  as.

with a skin depth  $\delta_L$ , and take a Gaussian XUV pulse with pulse length  $\tau_X = 300$  as.

Assuming free-electron dispersion,  $E = k^2/2$ , the energy-differential photoemission probability  $P(E, \tau) = \sum_{\varepsilon_n < \varepsilon_F} \left| \delta \tilde{\psi}_n(k, \tau) \right|^2$  leads to the delay-dependent center of energy (COE) of the PE spectrum

$$E_{COE}(\tau) = \frac{1}{2P_{tot}(\tau)} \sum_{\varepsilon_n < \varepsilon_F} \int dk \left| k \delta \tilde{\psi}_n(k, \tau) \right|^2, \quad (6)$$

where  $\delta \tilde{\psi}_n(k, \tau)$  is the Fourier transform of  $\delta \psi_n(z, t \rightarrow \infty; \tau)$  and  $P_{tot}(\tau) = \sum_{\varepsilon_n < \varepsilon_F} \int dk \left| \delta \tilde{\psi}_n(k, \tau) \right|^2$  the total emission probability.

In order to reveal the effect of the dynamic dielectric response on the streaked PE spectrum, we compare the results of two separate calculations for values of  $\hbar\omega_X$  between 30 and 100 eV. First, we solve (4) without  $\delta U(z, v_z)$  and denote the results as “static”. Next, we add wake effects and obtain “dynamic” results by including the real part of  $\delta U(z, v_z)$  in (4). In both calculations, we replace the imaginary part of  $\delta U(z, v_z)$  by the phenomenological expression  $\delta U_{ph}^i(z, v_z) = -v_z \Theta(-z)/(2\lambda)$  [26], where  $\lambda$  is the PE mean-free path.

We first present results for  $\delta_L = 0$  for which the IR field is completely screened inside the solid. Figure 2 compares the static and dynamic streaked PE spectra and their center of energies for  $\hbar\omega_X = 40$  eV. We define temporal shifts  $\tau_{sta(dyn)}$  for static (dynamic) calculations relative to  $A_L$  by fitting [18, 19]

$$E_{COE}^{sta(dyn)}(\tau) = a + bA_L(\tau - \Delta\tau_{sta(dyn)}). \quad (7)$$

Fig. 2(c) shows the relative temporal shift  $\Delta\tau_{wake} = \Delta\tau_{dyn} - \Delta\tau_{sta} \approx 100$  as, suggesting a noticeable - on the scale of the temporal resolution in measured streaked PE spectra - contribution of the dynamic plasmon response to the temporal shift.

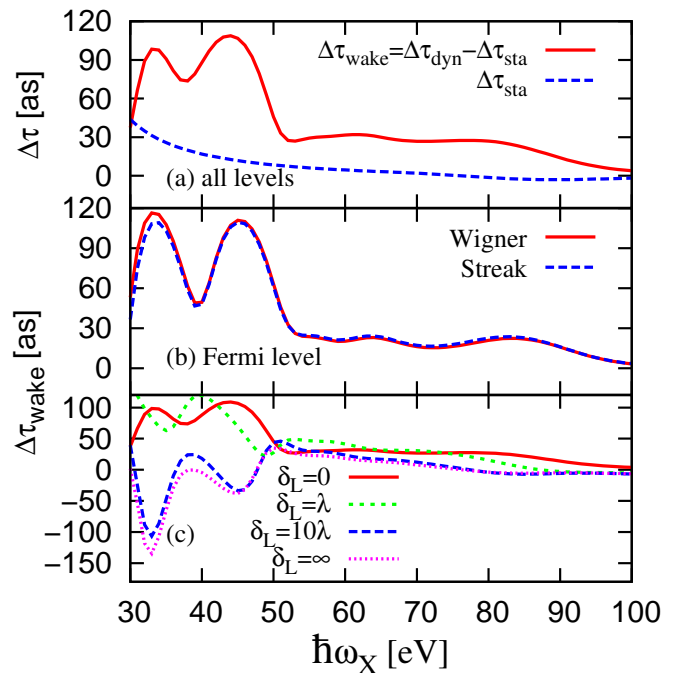


FIG. 3: (Color online) (a)  $\Delta\tau_{wake}$  and  $\Delta\tau_{sta}$  as a function of the XUV frequency obtained by fitting Eq. (7) to the calculated  $E_{COE}(\tau)$ , including all levels below the Fermi surface, for skin depth  $\delta_L = 0$ . (b) Comparison of  $\Delta\tau_{wake}$ , obtained from the streaked  $E_{COE}(\tau)$  at the Fermi surface, and the Wigner delay  $\Delta\tau_{wake}^W$ . (c)  $\Delta\tau_{wake}$  for different skin depths.

Our results for  $\Delta\tau_{dyn}$  and  $\Delta\tau_{sta}$  as a function of  $\hbar\omega_X$  in Fig. 3(a) reveal that the dynamic wake potential has a significant effect on the PE delay, especially for  $\hbar\omega_X < 50$  eV, where  $\Delta\tau_{dyn}$  develops a double-hump structure. The  $\hbar\omega_X$  dependence of  $\Delta\tau_{wake}$  can be understood as due to scattering of the PE in the wake potential  $\delta U(z, v_z)$ . This interaction of the PE with  $\delta U(z, v_z)$  changes the phase of  $\delta \psi_n(z, t)$ , giving rise to a Wigner delay  $\Delta\tau^W$  [27]. We determine  $\Delta\tau_{sta(dyn)}^W$  for  $A_L = 0$  by relating the PE position  $\langle z \rangle = \int dkz |\delta \psi_n(z, t)|^2$  and velocity  $\langle v \rangle = \int dk |k \delta \psi_n(k, t)|^2$  at a time  $t \gg \tau_L$  according to  $\langle z \rangle = \langle v \rangle (t - \Delta\tau^W)$ . In support of this “scattering interpretation”, Fig. 3(b) shows excellent agreement of the streaking delay  $\Delta\tau_{wake}$  with  $\Delta\tau_{wake}^W = \Delta\tau_{dyn}^W - \Delta\tau_{sta}^W$  for photoemission from the Fermi level. We find equally good agreement for emission from initial conduction band states below the Fermi level. For this comparison, we assumed that the IR field does not penetrate the solid ( $\delta_L = 0$ ).

Since the effect of the actual IR skin depth on the streaked spectrum from surfaces is currently debated [11, 18, 20–22], we found it compelling to study the influence of  $\delta_L$  on  $\Delta\tau_{wake}$ . Our numerical results in Fig. 3(c) show that  $\Delta\tau_{wake}$  is strongly affected by changes in the IR skin depth for  $\delta_L \lesssim 2\lambda$ , due to AC Stark polarization of the initial states  $\psi_n(z, t)$  and the PE wave packet  $\delta \psi_n(z, t)$ , as well as the combined action of  $U(z, v_z)$  and  $A_L(z, t)$  on  $\delta \psi_n(z, t)$  [19]. As contributions to the emit-

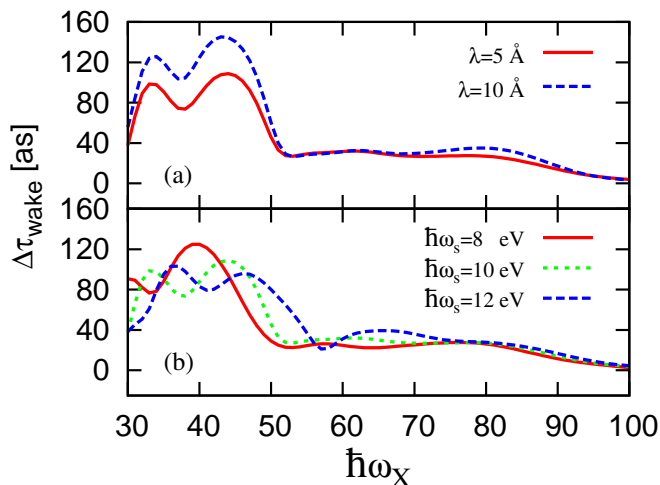


FIG. 4: (Color online) Relative delay  $\Delta\tau_{wake}$  as a function of the XUV frequency at different (a) PE mean-free paths and (b) surface plasmon frequencies.

ted photocurrent are limited to PEs that are released within a few mean-free paths  $\lambda$  from the surface,  $\Delta\tau_{wake}$  becomes less IR skin-depth dependent for  $\delta_L \gtrsim 2\lambda$  and stabilizes in the limit  $\delta_L \rightarrow \infty$ .

Figure 4 shows the dependence of  $\Delta\tau_{wake}$  on the PE mean free path and the surface plasmon frequency for  $\delta_L = 0$ . Increasing  $\lambda$  by a factor of two significantly increases  $\Delta\tau_{wake}$  for  $\hbar\omega_X \lesssim 50$  eV, but has little influence at larger  $\hbar\omega_X$  (Fig. 4(a)). Our result that, in general,  $\Delta\tau_{wake}(2\lambda) \neq \Delta\tau_{wake}(\lambda)$ , is incompatible with the interpretation [11, 22] of the delay between photoemission from core and conduction-band levels in tungsten being due solely to the PE's average travel time in the solid ( $\approx \lambda/\langle v \rangle$ ). Decreasing  $\omega_s$  shifts the double-hump structure to the lower  $\hbar\omega_X$ , and thus to lower kinetic energies of the PEs, as expected in view of the decreased thresholds for surface and bulk plasmon excitation (Fig. 4(b)).

In conclusion, we have calculated the wake potential induced in an aluminum surface by a PE that is released in the electric field of an attosecond XUV pulse. By comparing centers of energies and photoemission delays in IR-streaked PE spectra including the dynamic wake potential with calculations performed in the static limit, we find a significant contribution to the temporal shift  $\Delta\tau_{wake}$  in photoemission from the metal conduction band. This shift is due to the excitation of the bulk and surface plasmons in the metal during photoemission and is found to sensitively depend on the XUV frequency as well as on solid state characteristics, such as the bulk (surface) plasmon frequency, IR skin depth, and PE transport in the solid. The measurement of streaked electron spectra from dielectric solids, may thus be applied to probe solid state characteristic, in particular, the solid's ultra fast dielectric response to a moving charge with unprecedented accuracy. This is supported by our

quantitative prediction of wake-induced delays exceeding 50 as that fall within the temporal resolution achievable with contemporary laser technology [10].

This work was supported by the NSF, the Division of Chemical Sciences, Office of Basic Energy Sciences, Office of Energy Research, US DOE, and access to the Beocat computer cluster at Kansas State University.

- 
- [1] J. Harris and R. O. Jones, *J. Phys. C* **6**, 3585 (1973).
  - [2] J. R. Manson and R. H. Ritchie, *Phys. Rev. B* **24**, 4867 (1981).
  - [3] P. M. Echenique, F. Flore, and R. H. Ritchie, *Solid State Physics* **43**, 229 (1990).
  - [4] F. J. García de Abajo and P. M. Echenique, *Phys. Rev. B* **46**, 2663(1992); *Phys. Rev. B* **48**, 13399(1993).
  - [5] A. A. Lucas, E. Karthueser, and R. C. Badro, *Phys. Rev. B* **2**, 2488 (1970).
  - [6] M. Šunjić and A. A. Lucas, *Phys. Rev. B* **3**, 719 (1971).
  - [7] A. W. Overhauser, *Phys. Rev. B* **3**, 1888 (1971).
  - [8] J. Burgdörfer, *Nucl. Instrum. Methods* **24/25**, 139 (1987); C. O. Reinhold and J. Burgdörfer, *Phys. Rev. A* **55**, 450 (1997).
  - [9] J. I. Gersten and N. Tzoar, *Phys. Rev. B* **8**, 5671 (1973), N. Tzoar and J. I. Gersten, *Phys. Rev. B* **8**, 5684 (1973).
  - [10] M. Schultze *et al.*, *Science* **328**, 1658 (2010).
  - [11] A. L. Cavalieri *et al.*, *Nature* **449**, 1029 (2007).
  - [12] M. Drescher *et al.*, *Nature* **419**, 803 (2002).
  - [13] L. Miaja-Avila *et al.*, *Phys. Rev. Lett.* **101**, 046101 (2008).
  - [14] A. Kubo *et al.*, *Nano Lett.* **5**, 1123 (2005).
  - [15] M.I. Stockman *et al.*, *Nature Phot.* **1**, 539 (2007).
  - [16] M. Sukharev and T. Seideman, *Nano Lett.* **6**, 1123 (2006).
  - [17] F. Le *et al.*, *Phys. Rev. B* **76**, 165410 (2007); F. Hao *et al.*, *Phys. Rev. B* **76**, 165410 (2007).
  - [18] C.-H. Zhang and U. Thumm, *Phys. Rev. Lett.* **102**, 123601 (2009).
  - [19] C.-H. Zhang and U. Thumm, *Phys. Rev. A* **82**, 043405 (2010).
  - [20] J. C. Baggese and L. B. Madsen, *Phys. Rev. A* **78** 032903 (2008); *ibid.* **80** 030901(R) (2009).
  - [21] C. Lemell, B. Sollereder, K. Tökési, and J. Burgdörfer, *Phys. Rev. A* **79**, 062901 (2009).
  - [22] A. K. Kazansky and P. M. Echenique, *Phys. Rev. Lett.* **102** 177401 (2009).
  - [23] P. M. Echenique, R. H. Ritchie, N. Barberà, and J. Inkson, *Phys. Rev. B* **23**, 6486 (1981).
  - [24] H. Ibach, *Physics of Surfaces and Interfaces* (Springer-Verlag, Berlin, 2006).
  - [25] N. W. Ashcroft and N. D. Mermin, *Solid State Physics* (Thomson Learning, USA, 1976).
  - [26] The temporal shift calculated with  $\delta U^i$  is qualitatively equal to that obtained with the phenomenological imaginary potential  $\delta U_{ph}^i$  for  $\lambda = 5$  Å. Details on the quality of calculations with  $\delta U_{ph}^i$  will be published separately.
  - [27] C. A. A. de Carvalho and H. M. Nussenzweig, *Phys. Rep.* **364** 83 (2002).